Evaluation of PET Brain Radioligands for Imaging Pancreatic β-Cell Mass: Potential Utility of ^{11}C-(+)-PHNO

Jason Bini[1,2], Mika Naganawa[1], Nabeel Nabulsi[1], Yiyun Huang[1], Jim Ropchan[1], Keunpoong Lim[1], Soheila Najafzadeh[1], Kevan C. Herold[3], Gary W. Cline[3], and Richard E. Carson[1,2]

[1]PET Center, Yale University School of Medicine, New Haven, CT; [2]Department of Biomedical Engineering, Yale University, New Haven, CT; and [3]Department of Immunobiology and Internal Medicine, Yale University School of Medicine, New Haven, CT

Type 1 diabetes mellitus (T1DM) is characterized by a loss of β-cells in the islets of Langerhans of the pancreas and subsequent deficient insulin secretion in response to hyperglycemia. Development of an in vivo test to measure β-cell mass (BCM) would greatly enhance the ability to track diabetes therapies. β-cells and neurologic tissues have common cellular receptors and transporters, therefore, we screened brain radioligands for their ability to identify β-cells. **Methods:** We examined a β-cell gene atlas for endocrine pancreas receptor targets and cross-referenced these targets with brain radioligands that were available at our institution. Twelve healthy control subjects and 2 T1DM subjects underwent dynamic PET/CT scans with 6 tracers. **Results:** The D_2/D_3 receptor agonist radioligand ^{11}C-(+)-4-propyl-9-hydroxynaphthoxazine (PHNO) was the only radioligand to demonstrate sustained uptake in the pancreas with high contrast versus abdominal organs such as the kidneys, liver, and spleen, based on the first 30 min of data. Mean SUV from 20 to 30 min demonstrated high uptake of ^{11}C-(+)-PHNO in healthy controls (SUV, 13.8) with a 71% reduction in a T1DM subject with undetectable levels of C-peptide (SUV, 4.0) and a 20% reduction in a T1DM subject with fasting C-peptide level of 0.38 ng/mL (SUV, 11.0). SUV in abdominal organs outside the pancreas did not show measurable differences between the control and T1DM subjects, suggesting that the changes in SUV of ^{11}C-(+)-PHNO may be specific to changes in the pancreas between healthy controls and T1DM subjects. When D_3 and D_2 antagonists were used in nonhuman primates, specific pancreatic binding (SUVR-1) of ^{11}C-PHNO was reduced by 57% and 38%, respectively. **Conclusion:** ^{11}C-(+)-PHNO is a potential marker of BCM, with 2:1 binding of D_3 receptors over D_2 receptors. Further in vitro and in vivo studies to establish D_2/D_3 receptor specificity to β-cells is warranted to characterize ^{11}C-(+)-PHNO as a candidate for clinical measurement of BCM in healthy control and diabetic subjects.

Key Words: diabetes; pancreas; β-cell mass; PHNO; PET

J Nucl Med 2018; 59:1249–1254
DOI: 10.2967/jnumed.117.197285

Type 1 diabetes mellitus (T1DM) is characterized by a loss of β-cells in the islets of Langerhans of the pancreas and the subsequent inability to secrete insulin in response to hyperglycemia (*1*). Current understanding of how the loss of β-cell mass (BCM) contributes to loss of function has been largely determined from postmortem analysis. In the absence of clinically validated methods to measure BCM in vivo, functional studies have been used as a surrogate. However, functional studies, such as C-peptide levels, a measure of endogenous insulin production by β-cells, can be affected by factors including fatty acids, insulin resistance, and even glucose itself. Current tests, such as the oral glucose tolerance test, may not accurately correlate with BCM due to β-cells that are not responsive to stimuli but may still be viable and responsive to treatment. In addition, the sensitivity of β-cells to provocative stimuli may change during different stages of diabetes (*2–4*). Therefore, development of techniques to measure BCM in vivo would greatly enhance the ability to simultaneously track changes in BCM and function, and to evaluate the efficacy and mechanisms of therapies to preserve or restore insulin secretion (*5*). Several modalities have been proposed for imaging BCM such as PET, SPECT, MRI, and optical methods (*6*).

Previous PET studies have attempted to measure BCM by targeting receptors specific to the endocrine pancreas (*7–16*). Two radioligands with promising results were ^{18}F-FP-(+)-dihydrotetrabenazine (DTBZ), which targets vesicular monoamine transporter 2 (VMAT2) and colocalizes with insulin secretory vesicles (*7–9,11*), and ^{11}C-5-hydroxytryptophan (5HTP), a precursor of serotonin present in β-cells that may be involved in insulin secretion (*10,12,14*). For ^{18}F-FP-(+)-DTBZ, binding may not be entirely specific to β-cells as there is some evidence of binding in polypeptide cells (*17*). For ^{11}C-5HTP, despite demonstrating binding in the islets of Langerhans, it is not clear that binding was specific to β-cells and not due to other endocrine cells (*10,12,14*). Dopamine, cosecreted with insulin, may act as an autocrine signal via its binding to dopamine receptors (DRs) on the surface of β-cells and thus may be a useful target (*18,19*).

β-cells and neurologic tissues have common cellular receptors and transporters, and therefore, we screened other brain radioligands for their ability to identify β-cells. We used a β-cell gene atlas to identify possible endocrine pancreas receptor targets and cross-referenced these targets with PET brain radioligands that were available at our institution. Existing radioligands were then examined for high pancreatic uptake and high contrast to neighboring organs to determine which radioligands warranted further study. Those radioligands that exhibited such features were tested in T1DM subjects and nonhuman primates (NHPs).

MATERIALS AND METHODS

Subjects

Twelve healthy control (HC) subjects (6 male/6 female) and 2 male T1DM subjects were included in the study. The average age and weight were 33 ± 9 y and 76 ± 12 kg, respectively. Diabetes duration, at the

Received Jun. 9, 2017; revision accepted Dec. 7, 2017.
For correspondence or reprints contact: Jason Bini, Yale University, 801 Howard Ave., P.O. Box 208048, New Haven, CT 06520.
Email: jason.bini@yale.edu
Published online Jan. 25, 2018.

TABLE 1
Injected Doses and Mass (Minimum–Maximum) for Radioligands and Respective Targets in Human Studies

Radioligand	Radioligand target	Injected dose (MBq)	Injected mass (μg)
^{11}C-(+)-PHNO	D_2/D_3 receptors	209–351	1.63–2.30
^{11}C-FLB457	D_2/D_3 receptors	326–344	0.59–0.60
^{11}C-raclopride	D_2/D_3 receptors	272–346	0.45–3.27
^{11}C-DASB	Serotonin transporter	166–359	0.25–0.61
^{11}C-AS2471907	11β-HSD1 enzyme inhibitor	208–214	2.75–3.00
^{11}C-UCB-J	Synaptic vesicle protein 2A	46–322	1.00–1.49

Two subjects (1 male/1 female) were scanned for each radioligand with exception of ^{11}C-(+)-PHNO ($n = 4$).

time of scanning, for T1DM subjects was 29 y (fasting C-peptide undetectable) and 14 y (fasting C-peptide, 0.38 ng/mL); all HCs were screened to exclude existing diabetes (normal fasting C-peptide range, 0.8–3.1 ng/mL). The study was approved by the Yale University Institutional Review Board and Radiation Safety Committees, and all subjects signed a written informed consent form.

β-Cell Gene Atlas Screening

We cross-referenced the targets of available radioligands at the Yale PET Center with a β-cell gene atlas to find radioligands that may be useful BCM biomarkers (*20*). Relative Affymetrix β-cell gene expression is defined on a 0–100 scale (0–25, no expression; 25–50, low; 50–75, moderate; and 75–100, enriched). All radioligands with a relative expression of 50 or more (moderate or enriched expression) were considered potentially useful.

Human Imaging

On the basis of the gene atlas, we chose 6 radioligands for evaluation. Human PET/CT imaging was performed on a Biograph mCT-X PET/CT system (Siemens Healthcare). A 30-min dynamic scan (6 × 30, 3 × 60, 2 × 120, and 4 × 300 s) centered on the pancreas was performed followed by a 30-min whole-body acquisition (2 passes, 120 s per bed position) followed by an additional 60-min dynamic scan (12 × 300 s) at the level of the pancreas. Injected doses and mass for each radioligand are provided in Table 1. Dynamic scans were reconstructed using an ordered-subset expectation maximization–based algorithm with point-spread function and time-of-flight correction. Attenuation correction was performed using the CT acquisition. Regions of interest (ROIs) were drawn manually on a summed image (0–10 min), then eroded to avoid partial-volume effects, for the pancreas, liver, kidneys, and spleen, and time–activity curves were produced in SUV units. SUV and SUV ratio (SUVR, spleen as reference) (*13*) were calculated on summed images (20–30 min). No respiratory motion correction was performed; a previous study demonstrated an underestimation of only 15% ± 6% in noncorrected scans for ^{18}F-FP-(+)-DTBZ (*21*).

NHP Imaging

NHP studies were performed to evaluate D_2- and D_3-specific binding components in the pancreas. A NHP (age, 13 y; weight, 20.9 kg) underwent scans on 2 separate days, with 2 scans per day: baseline followed by a blocking scan with tracer injections separated by 4 h. Mean injected doses were 182 ± 1 MBq, and mass was 0.64 ± 0.10 μg. The blocking scans began 30 min after an infusion of D_3-selective antagonist SB277011A (0.3 mg/kg) and D_2-selective antagonist L-741,626 (1 mg/kg). Acquisitions on the mCT-X included a 30-min dynamic scan (6 × 30, 3 × 60, 2 × 120, and 4 × 300 s) centered on the pancreas followed by a 4-bed (3 min/bed) whole-body acquisition with 3 passes from head to thigh (36 min total). ROIs were drawn manually on a summed image from 0 to 10 min for the pancreas and spleen. Mean pancreatic SUV and SUVR (spleen as reference) from 20 to 30 min were calculated. Binding potential (BP_{ND}) was calculated in the pancreas using simplified reference tissue model (SRTM).

TABLE 2
Radioligand Target Relative Gene Expression with Rankings of 0–100 Gathered from β-Cell Gene Atlas (*20*)

Radioligand	Gene expression			
	Gene	Human exocrine pancreas	Human pancreatic islets	Human primary β-cells*
^{11}C-(+)-PHNO, ^{11}C-FLB457, ^{11}C-raclopride	DRD2	63	55	74*
	DRD3*	1*	4*	69*
^{11}C-DASB	SLC6A4	59	69	54*
^{11}C-AS2471907	HSD11B1	44	75	48*
^{11}C-UCB-J	SV2A	16	72	86*

*Retrospective analysis for relative gene expression was examined after completion of PET scans to provide insight into differences of pancreas uptake among the 3 D_2/D_3 receptor radioligands (^{11}C-raclopride, ^{11}C-FLB457, and ^{11}C-(+)-PHNO). DRD2 = dopamine receptor 2; DRD3 = –dopamine receptor 3; SLC6A4 = serotonin transporter; HSD11B1 = 11β-hydroxysteroid dehydrogenase type 1 enzyme inhibitor; SV2A = synaptic vesicle protein 2A.

Expression group rankings: none (0–25), low (25–50), moderate (50–75), enriched (75–100).

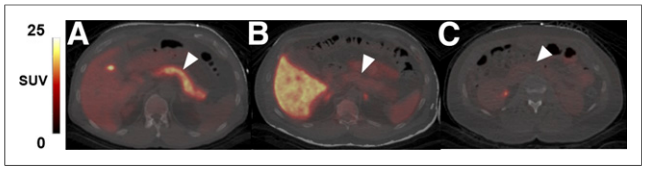

FIGURE 1. Representative axial slices of PET/CT overlay of pancreas uptake (arrowheads) for each dopaminergic radioligand ^{11}C-(+)-PHNO (A), ^{11}C-FLB457 (B), and ^{11}C-raclopride (C). All SUV images summed from 20 to 30 min.

In the brain, substantia nigra (SN), caudate, and putamen ROIs were defined from a brain atlas (*22*) coregistered to the image (30–60 min), and SUV and SUVR (cerebellum as reference) were determined. Using SUVR-1 as a measure of specific binding, we determined percentage reduction in specific pancreatic and brain binding due to the blocking drugs.

To confirm the use of SUVR-1 in blocking studies, we used brain modeling methods in a second NHP (age, 17 y; weight, 14.5 kg) with baseline and blocking brain scans on the Focus 220 (Siemens) with only L-741,626, using the same timing and doses as above. As in previous studies, time–activity curves were generated for brain ROIs, BP_{ND} was calculated using SRTM2 (*22–24*), and regional occupancy was calculated.

RESULTS

We identified 6 potentially useful radioligands targeting 4 different receptor sites: ^{11}C-raclopride, ^{11}C-FLB457, and ^{11}C-(+)-4-propyl-9-hydroxynaphthoxazine (PHNO), and ^{11}C-(+)-PHNO (D_2/D_3 receptors); ^{11}C-DASB (serotonin transporter); ^{11}C-AS247190 (11β-hydroxysteroid dehydrogenase type 1 (HSD1) enzyme inhibitor) (*25*); and ^{11}C-UCB-J (synaptic vesicle protein 2A) (*26,27*). Relative gene expressions of these targets are provided in Table 2. Initially, for β-cell gene expression screening, only the D_2 receptor gene was used to identify potential dopaminergic ligands because all D_2/D_3 radioligands (^{11}C-raclopride, ^{11}C-FLB457, and ^{11}C-(+)-PHNO) target D_2 receptors to some extent, although with varying affinities for each receptor. ^{11}C-raclopride and ^{11}C-FLB457 are both receptor antagonists; however, ^{11}C-raclopride (*28*) has lower affinity than ^{11}C-FLB457 (*29*). ^{11}C-(+)-PHNO is an agonist with 25- to 50-fold-higher affinity for D_3 receptors (*22*). Retrospective analysis after completion of PET scans to provide insight into differences between the dopaminergic radioligands included the D_3 receptor gene and the addition of the Human Primary β-Cells column (Table 2).

^{11}C-(+)-PHNO was the only dopaminergic radioligand to demonstrate sustained uptake in the pancreas, with high contrast to the kidneys, liver, and spleen, based on SUV images (20–30 min) and time–activity curves (0–30 min). Representative PET images (Fig. 1) and time–activity curves (Fig. 2) of the 3 D_2/D_3 radioligands demonstrated the apparent superiority of ^{11}C-(+)-PHNO.

TABLE 3
Pancreatic SUV (20–30 Minutes) of Each Radioligand in HCs (SUVR, Spleen Reference)

Radioligand	Pancreas (SUV)	Pancreas/spleen (SUVR)
^{11}C-(+)-PHNO	13.8 ± 1.7	7.1 ± 0.4
^{11}C-FLB457	3.0 ± 0.8	0.9 ± 0.0
^{11}C-raclopride	2.2 ± 0.5	1.4 ± 0.0
^{11}C-DASB	4.0 ± 0.6	0.7 ± 0.1
^{11}C-AS2471907	0.6 ± 0.1	0.4 ± 0.1
^{11}C-UCB-J	1.6 ± 0.4	1.7 ± 0.3

Data are mean ± SD.

Low pancreas SUV and SUVR were seen in all other radioligands compared with ^{11}C-(+)-PHNO (Table 3) as seen in representative PET images (Supplemental Fig. 1; supplemental materials are available at http://jnm.snmjournals.org) and time–activity curves (Supplemental Fig. 2). Time–activity curves (0–90 min) showed no contrast in the pancreas compared with reference organ (spleen) beyond 30 min for any radioligand.

^{11}C-(+)-PHNO pancreas SUV was 13.8 ± 1.7 in HCs. A 71% reduction (SUV, 4.0) was seen in the T1DM subject with undetectable C-peptide levels. In a T1DM subject with a fasting C-peptide level of 0.38 ng/mL, a 20% reduction (SUV, 11.0) was seen (Fig. 3; Table 4). Comparisons between time–activity curves of the C-peptide–deficient T1DM subject demonstrated substantially reduced uptake and contrast to background organs compared with the HCs (Fig. 4). SUV in other abdominal organs did not show differences between HC and T1DM (Table 5), suggesting that the ^{11}C-(+)-PHNO SUV differences are specific to changes in the pancreas.

Assessing the D_2 and D_3 components of ^{11}C-(+)-PHNO–specific binding, SUVR-1 and BP_{ND} of ^{11}C-(+)-PHNO in NHP was reduced by a D_3 receptor antagonist in the pancreas, SN, putamen, and caudate (Table 5; Supplemental Fig. 3). SUVR-1 and BP_{ND} for the D_2 receptor antagonist demonstrated a smaller reduction than the D_3 receptor antagonist in the pancreas and SN and larger reductions in the putamen and caudate (Table 5). When a brain-only study was performed, BP_{ND} demonstrated reductions in the SN, putamen, and caudate similar to SUVR-1 in the previous D_2 antagonist multiorgan scan (Table 5; Supplemental Fig. 4), suggesting that SUVR-1 is a valid measure for assessing blockade.

The SN can be considered approximately 100% D_3-selective, and the putamen and caudate about 100% D_2-selective. Because the pancreas blocking percentages fell between the values for these regions, this suggests that ^{11}C-PHNO binds to both D_2 and D_3 in the pancreas.

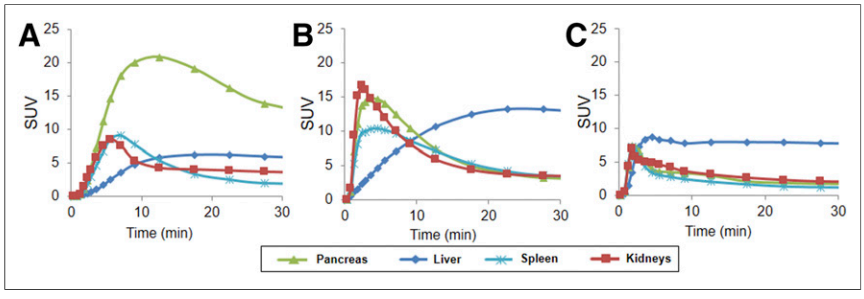

FIGURE 2. Mean time–activity curves of pancreas, liver, spleen, and kidneys of 2 HCs for each dopaminergic radioligand ^{11}C-(+)-PHNO (A), ^{11}C-FLB457 (B), and ^{11}C-raclopride (C).

DISCUSSION

We identified 6 radioligands through use of a β-cell gene atlas that were subsequently screened using PET/CT in HCs for high pancreas uptake and high

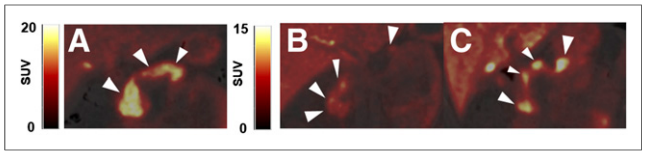

FIGURE 3. Representative coronal PET/CT images of ^{11}C-(+)-PHNO in pancreas (arrowheads) for HC (A), C-peptide–deficient T1DM subject (B), and T1DM subject with detectable C-peptide (C). All SUV images are summed from 20 to 30 min. (A) SUV scale 0–20. (B and C) SUV scale 0–15.

contrast-to-background abdominal organs, similar to a previous study (*12*). The D_3-preferring radioligand ^{11}C-(+)-PHNO showed the best potential as a BCM-imaging agent, based on high pancreatic uptake in HCs, lower uptake in T1DM subjects, and demonstrable specific binding with NHP blocking studies.

Of the 6 radioligands studied, 3, ^{11}C-UCB-J (synaptic vesicle protein 2A), ^{11}C-DASB (serotonin transporter), and ^{11}C-AS2471907 (11β-HSD1 enzyme inhibitor), did not demonstrate high pancreas signal or contrast-to -background abdominal organs (Table 3). Synaptic vesicle proteins are associated with insulin-containing granules in neuroendocrine cells (*30,31*); however, evoked basal hormone release was attenuated more by silencing SV2C than SV2A in neuroendocrine cells, possibly explaining low SV2A signal (*31*). The main mechanism of 11β-HSD1 inhibition is lowering intracellular cortisol concentrations in the liver and adipose tissue, and liver uptake was more than 25 times that of the pancreas, making ^{11}C-AS2471907 undesirable for BCM imaging (*32*). Serotonin mechanisms have been implicated in the endocrine pancreas (*10,33*); however, given low uptake and contrast in the pancreas, ^{11}C-DASB may not be a suitable BCM imaging agent.

In agreement with studies suggesting the feasibility of targeting DRs for imaging BCM (*15,16,19*), promising results were obtained for 1 of the 3 DR radioligands. ^{11}C-(+)-PHNO demonstrated the greatest uptake and contrast compared with background organs in HCs. In contrast, a large reduction in SUV (71%) in the pancreas of a subject with T1DM without detectable C-peptide (Table 4) suggests possible specific binding of ^{11}C-(+)-PHNO to islet β-cells. Intriguingly, a T1DM subject with detectable levels of insulin production had higher pancreas SUV than the first T1DM subject (Table 3), suggestive of intermediate BCM levels.

Using the 3 dopaminergic radioligands in our study, we can indirectly infer mechanisms of both D_2 and D_3 receptors. On the basis of preliminary success with D_2 receptor radioligands to differentiate healthy and diabetic rats (*15,16*), and the β-cell gene atlas data (Table 2), D_2 receptors may exist throughout the endocrine and exocrine pancreas. D_2 receptors, as measured by ^{11}C-(+)-PHNO, may not be directly or linearly correlated with β-cells; therefore, information obtained by this imaging technique should be viewed with caution. Further study is required to assess whether reduced D_3 receptors in T1DM are specific to human β-cells.

^{11}C-raclopride and ^{11}C-FLB457 are both antagonists, and thus have equal affinity for high- and low-affinity receptor sites; ^{11}C-FLB457 has higher affinity (*29,34*). ^{11}C-(+)-PHNO is an agonist that binds to D_2 and D_3 receptors with a 25- to 50-fold-higher affinity for D_3 receptors. Quelch et al., reported higher specific binding with [^{3}H](+)PHNO versus [^{3}H]raclopride in microsomal but not extracellular or cytosolic tissue in the pig striatum (*35*). Similar $D_{2/3}$ receptor internalization may occur in the pancreas, which may explain the higher binding of ^{11}C-(+)-PHNO than ^{11}C-raclopride or ^{11}C-FLB457.

To assess the D_2 and D_3 components of pancreatic ^{11}C-(+)-PHNO binding, we performed blocking experiments in NHP. The brain occupancy data for the D_3 antagonist agreed well with previous ^{11}C-(+)-PHNO data (*36*). For each blocking study (Table 5), using the receptor occupancy values in pancreas (r_{panc}), putamen (r_{put}), and SN (r_{SN}), and assuming that SN and putamen are 100% D_3- and D_2-selective, respectively, we can estimate the fraction of D_3 (f_{D3}) and D_2 (1-f_{D3}) binding in the pancreas (the supplemental materials provide a derivation of the equation):

$$f_{D3} = \frac{r_{panc} - r_{put}}{r_{SN} - r_{put}} \qquad \text{Eq. 1}$$

In the D_2 antagonist–blocking study, f_{D3} is 0.77 using SUVR-1 or BP_{ND} and in the D_3-blocking study, f_{D3} is 0.58 (SUVR-1) or 0.43 (BP_{ND}). Averaging suggests that specific binding in the pancreas is about two-thirds D_3 and one-third D_2. Note that because specific binding measurements at tracer levels represent receptor density (B_{max})/affinity (K_d), not B_{max}, this does not imply that two-thirds of the $D_{2/3}$ receptors are D_3. Rather, if the relative D_2/D_3 affinities for ^{11}C-(+)-PHNO in the pancreas are the same as those in the brain, that is, a 25- to 50-fold-higher affinity for D_3 (*22*), then the B_{max} for D_2 is in fact much higher than that of D_3.

The connection between dopaminergic activity and the endocrine pancreas has been known for 40 y (*37,38*). It is believed that circulating dopamine is generally below levels needed to activate peripheral DRs (*39*). One current theory proposes that circulating L-DOPA (dopamine precursor) is taken up by β-cells, converted to dopamine, and cosecreted with insulin as an autocrine signal by binding to DRs on the surface of β-cells (*19*). Dopamine antagonists have been shown to cause hyperinsulinemia in healthy subjects and are associated with diabetes in psychiatric patients, versus agonists such as bromocriptine, which improved glycemic control (*40*). Interestingly, L-DOPA, a common treatment in Parkinson

TABLE 4
SUV (20–30 Minutes) of ^{11}C-(+)-PHNO in Pancreas, Spleen, Kidneys, and Liver

^{11}C-(+)-PHNO	Pancreas/spleen (SUVR)	Pancreas (SUV)	Spleen (SUV)	Kidneys (SUV)	Liver (SUV)
HCs (n = 2)	7.1 ± 0.4	13.8 ± 1.7	2.0 ± 0.3	5.9 ± 3.0	7.2 ± 1.7
T1DM (n = 2)	2.1*, 4.4†	4.0*, 11.0†	2.2 ± 0.4	5.0 ± 0.4	7.8 ± 1.6

*Undetectable C-peptide T1DM subject.
†Detectable C-peptide T1DM subject.
Data are mean ± SD.

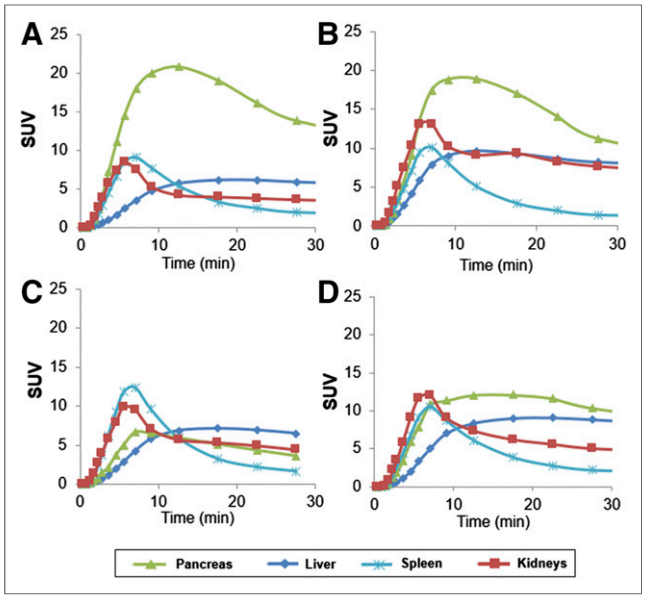

FIGURE 4. ^{11}C-(+)-PHNO time–activity curves of pancreas, liver, spleen, and kidneys for HCs (A and B), C-peptide–deficient T1DM (C), and T1DM subject with detectable C-peptide (D).

disease, has demonstrated reduced insulin secretion in such patients and mice (*40*). Combined, this evidence suggests dopamine may be an integral part of the endocrine pancreas.

Several studies have attempted to elucidate more specific mechanisms of DRs in the endocrine pancreas. In vitro studies using mouse islet cells have indicated that a D_3 receptor antagonist increases insulin secretion, suggesting that dopamine binding to the D_3 receptor inhibits insulin secretion (*18*). In contrast, Chen et al. found no evidence of pancreatic D_3 receptors in rats using Western blot and immunofluorescence techniques, and concluded D_1 receptors were colocalized with insulin staining in rat Islet cells (*41*). Additional studies have indicated the D_2 receptor may be involved in insulin secretion inhibition (*42–45*). Several other studies have demonstrated inhibitory actions of dopamine on insulin release in preclinical models but did not assess whether specific receptors were responsible for such actions (*37,46–49*). It is important to note that the structure and function of proteins may differ between species such as mouse, rat, and in vitro cultures of insulinoma cell lines, such as INS-1 cells. The human β-cell gene expression atlas we used demonstrated a specificity of the D_3 receptor gene to β-cells and lack of expression in the exocrine and other endocrine cells in the islets of Langerhans (Table 2) (*20*). Further studies are warranted to determine the specificity of different DR subtypes in the endocrine pancreas and β-cells. However, from this evidence and the large reduction seen in the T1DM subject with undetectable C-peptide, we hypothesize that high-affinity D_3 receptors may be specific to the endocrine pancreas and perhaps to β-cells.

Several potential limitations in the current study must be assessed. The use of spleen as a reference region has been examined for the VMAT2 tracer ^{18}F-FP-(+)-DTBZ (*13*) and we used SUVR in the current study. Several issues must be evaluated to validate this choice. First, the presence of D_2/D_3 receptors in the spleen must be assessed; a preliminary study has demonstrated that all 5 DR subtypes, along with VMAT1 and VMAT2, are present to some extent in the spleen (*50*). In NHP blocking studies, we saw 37% and 13% reductions in spleen SUV during D_2 and D_3 antagonist studies, respectively; however, no differences were seen between HC and T1DM subjects in spleen SUV. Second, it remains to be validated if nondisplaceable binding in the spleen is equal to the pancreas, or if a scale-factor correction is needed, as with the VMAT2 tracer (*13*). Further, radiolabeled metabolites may accumulate in the spleen; therefore, we focused on early data (20–30 min) for the patient comparisons, to maximize specific binding while simultaneously minimizing potential biases due to radiolabeled metabolites. Arterial sampling of HC and T1DM subjects should be performed to characterize ^{11}C-(+)-PHNO metabolites and assess whether there are between-group differences that may affect interpretation of results, similar to a previous study with enantiomers of ^{18}F-FP-DTBZ (*13*).

CONCLUSION

We have examined 6 PET brain radioligands in the pancreas in both HC and T1DM subjects and have demonstrated that ^{11}C-(+)-PHNO, a D_3-preferring receptor agonist, may be a potential marker of BCM. NHP blocking studies suggest that about two-thirds of pancreatic binding originates from D_3 receptors. Further in vitro and in vivo studies to establish D_3 receptor specificity to β-cells are warranted to develop ^{11}C-(+)-PHNO as a candidate for clinical measurement of BCM.

TABLE 5
SUVR-1 and BP_{ND} in Baseline and Blocking Scans, and Percentage Reduction from Baseline in Pancreas and Brain Regions in NHPs with ^{11}C-(+)-PHNO

Antagonist	Measure	Pancreas	Substantia nigra	Putamen	Caudate
D_3	SUVR-1	2.8/1.2/57%	2.8/0.3/89%	4.7/4.1/13%	3.7/2.9/22%
	BP_{ND}	1.5/0.8/46%	*	*	*
D_2	SUVR-1	1.6/1.0/38%	4.0/3.0/25%	5.8/1.1/81%	5.2/1.4/73%
	BP_{ND}	0.8/0.5/38%	*	*	*
D_2	BP_{ND}	*	3.5/2.7/23%	4.3/0.9/79%	4.3/0.9/79%

*Dynamic data not available.

Data are presented as baseline values/blocking values/percentage reduction. BP_{ND} calculated using SRTM for pancreas (spleen reference) and SRTM2 for brain (cerebellum reference).

DISCLOSURE

This study was supported by the NIH grant 1DP3DK104092-01 and was also made possible by 1S10OD010322-01 and by CTSA grant number UL1 TR000142 from the National Center for Advancing Translational Sciences (NCATS), a component of the NIH. Its contents are solely the responsibility of the authors and do not necessarily represent the official view of the NIH. No other potential conflict of interest relevant to this article was reported.

ACKNOWLEDGMENTS

The authors appreciate the excellent technical assistance of the Yale PET Center staff.

REFERENCES

1. Steele C, Hagopian W, Gitelman S, et al. Insulin secretion in type 1 diabetes. *Diabetes.* 2004;53:426–433.
2. Meier JJ, Menge B, Breuer TGK, et al. Functional assessment of pancreatic β-cell area in humans. *Diabetes.* 2009;58:1595–1603.
3. Meier JJ, Bonadonna RC. Role of reduced β-cell mass versus impaired β-cell function in the pathogenesis of type 2 diabetes. *Diabetes Care.* 2013;36 (suppl 2):S113–S119.
4. Weir GC, Bonner-Weir S. Sleeping islets and the relationship between β-cell mass and function. *Diabetes.* 2011;60:2018–2019.
5. Weir GC, Bonner-Weir S. Islet β-cell mass in diabetes and how it relates to function, birth, and death. *Ann N Y Acad Sci.* 2013;1281:92–105.
6. Jodal A, Schibli R, Béhé M. Targets and probes for non-invasive imaging of β-cells. *Eur J Nucl Med Mol Imaging.* 2017;44:712–727.
7. Goland R, Freeby M, Parsey R, et al. ^{11}C-dihydrotetrabenazine PET of the pancreas in subjects with long-standing type 1 diabetes and in healthy controls. *J Nucl Med.* 2009;50:382–389.
8. Singhal T, Ding YS, Weinzimmer D, et al. Pancreatic beta-cell mass PET imaging and quantification with [^{11}C]DTBZ and [^{18}F]FP-(+)-DTBZ in rodent models of diabetes. *Mol Imaging Biol.* 2011;13:973–984.
9. Normandin MD, Petersen KF, Ding Y-S, et al. In vivo imaging of endogenous pancreatic β-cell mass in healthy and type 1 diabetic subjects using ^{18}F-fluoropropyl-dihydrotetrabenazine and PET. *J Nucl Med.* 2012;53:908–916.
10. Eriksson O, Espes D, Selvaraju RK, et al. Positron emission tomography ligand [^{11}C]5-hydroxy-tryptophan can be used as a surrogate marker for the human endocrine pancreas. *Diabetes.* 2014;63:3428–3437.
11. Freeby MJ, Kringas P, Goland RS, et al. Cross-sectional and test-retest characterization of PET with [^{18}F]FP-(+)-DTBZ for β-cell mass estimates in diabetes. *Mol Imaging Biol.* 2016;18:292–301.
12. Karlsson F, Antonodimitrakis PC, Eriksson O. Systematic screening of imaging biomarkers for the Islets of Langerhans, among clinically available positron emission tomography tracers. *Nucl Med Biol.* 2015;42:762–769.
13. Naganawa M, Lin S-F, Lim K, et al. Evaluation of pancreatic VMAT2 binding with active and inactive enantiomers of ^{18}F-FP-DTBZ in baboons. *Nucl Med Biol.* 2016;43:743–751.
14. Carlbom L, Espes D, Lubberink M, et al. [^{11}C]5-hydroxy-tryptophan PET for assessment of islet mass during progression of type 2 diabetes. *Diabetes.* 2017;66:1286–1292.
15. Garcia A, Venugopal A, Pan M-L, Mukherjee J. Imaging pancreas in healthy and diabetic rodent model using [^{18}F]fallypride positron emission tomography/computed tomography. *Diabetes Technol Ther.* 2014;16:640–643.
16. Willekens SMA, Van Der Kroon I, Joosten L, et al. SPECT of transplanted Islets of Langerhans by dopamine 2 receptor targeting in a rat model. *Mol Pharm.* 2016;13:85–91.
17. Saisho Y, Harris PE, Butler AE, et al. Relationship between pancreatic vesicular monoamine transporter 2 (VMAT2) and insulin expression in human pancreas. *J Mol Histol.* 2008;39:543–551.
18. Ustione A, Piston DW. Dopamine synthesis and D3-receptor activation in pancreatic β-cells regulates insulin secretion and intracellular [Ca^{2+}] oscillations. *Mol Endocrinol.* 2012;26:1928–1940.
19. Ustione A, Piston DW, Harris PE. Minireview: dopaminergic regulation of insulin secretion from the pancreatic islet. *Mol Endocrinol.* 2013;27:1198–1207.
20. Kutlu B, Burdick D, Baxter D, et al. Detailed transcriptome atlas of the pancreatic beta-cell. *BMC Med Genomics.* 2009;2:1–11.
21. Ren S, Jin X, Chan C, et al. Data-driven respiratory motion estimation and correction using TOF PET list-mode centroid of distribution. *Phys Med Biol.* 2017;62:4741–4755.
22. Gallezot JD, Beaver JD, Gunn RN, et al. Affinity and selectivity of [^{11}C]-(+)-PHNO for the D3 and D2-receptors in the rhesus monkey brain in vivo. *Synapse.* 2012;66:489–500.
23. Innis RB, Cunningham VJ, Delforge J, et al. Consensus nomenclature for in vivo imaging of reversibly binding radioligands. *J Cereb Blood Flow Metab.* 2007;27:1533–1539.
24. Wu Y, Carson RE. Noise reduction in the simplified reference tissue model for neuroreceptor functional imaging. *J Cereb Blood Flow Metab.* 2002;22:1440–1452.
25. Huang Y, Planet B, Nabulsi N, et al. First-in-human study of the 11{beta}-hydroxysteroid dehydrogenase type 1 PET tracer [^{11}C]AS2471907 [abstract]. *J Nucl Med.* 2016;57:580.
26. Nabulsi NB, Mercier J, Holden D, et al. Synthesis and preclinical evaluation of ^{11}C-UCB-J as a PET tracer for imaging the synaptic vesicle glycoprotein 2A in the brain. *J Nucl Med.* 2016;57:777–784.
27. Finnema SJ, Nabulsi NB, Eid T, et al. Imaging synaptic density in the living human brain. *Sci Transl Med.* 2016;8:348ra96-348ra96.
28. Farde L, Eriksson L, Blomquist G, Halldin C. Kinetic analysis of central [^{11}C]raclopride binding to D2-dopamine receptors studied by PET: a comparison to the equilibrium analysis. *J Cereb Blood Flow Metab.* 1989;9:696–708.
29. Halldin C, Farde L, Högberg T, et al. Carbon-11-FLB 457: a radioligand for extrastriatal D2 dopamine receptors. *J Nucl Med.* 1995;36:1275–1281.
30. Portela-Gomes GM, Lukinius A, Grimelius L. Synaptic vesicle protein 2, a new neuroendocrine cell marker. *Am J Pathol.* 2000;157:1299–1309.
31. Iezzi M, Theander S, Janz R, et al. SV2A and SV2C are not vesicular Ca2+ transporters but control glucose-evoked granule recruitment. *J Cell Sci.* 2005; 118:5647–5660.
32. Pereira CD, Azevedo I, Monteiro R, Martins MJ. 11β-hydroxysteroid dehydrogenase type 1: relevance of its modulation in the pathophysiology of obesity, the metabolic syndrome and type 2 diabetes mellitus. *Diabetes Obes Metab.* 2012;14:869–881.
33. Eriksson O, Selvaraju RK, Johansson L, et al. Quantitative imaging of serotonergic biosynthesis and degradation in the endocrine pancreas. *J Nucl Med.* 2014;55:460–465.
34. Seeman P. Antipsychotic drugs, dopamine receptors, and schizophrenia. *Clin Neurosci Res.* 2001;1:53–60.
35. Quelch DR, Withey SL, Nutt DJ, et al. The influence of different cellular environments on PET radioligand binding: an application to D2/3-dopamine receptor imaging. *Neuropharmacology.* 2014;85:305–313.
36. Rabiner EA, Slifstein M, Nobrega J, et al. In vivo quantification of regional dopamine-D3 receptor binding potential of (+)-PHNO: Studies in non-human primates and transgenic mice. *Synapse.* 2009;63:782–793.
37. Ericson LE, Håkanson R, Lundquist I. Accumulation of dopamine in mouse pancreatic β-cells following injection of L-DOPA localization to secretory granules and inhibition of insulin secretion. *Diabetologia.* 1977;13:117–124.
38. Leblanc H, Lachelin GCL, Yen SSC, et al. The effect of dopamine infusion on insulin and glucagon secretion in man. *J Clin Endocrinol Metab.* 1977;44:196–198.
39. Goldstein DS, Eisenhofer G, Kopin IJ. Sources and significance of plasma levels of catechols and their metabolites in humans. *J Pharmacol Exp Ther.* 2003;305:800–811.
40. Lopez Vicchi F, Luque GM, Brie B, et al. Dopaminergic drugs in type 2 diabetes and glucose homeostasis. *Pharmacol Res.* 2016;109:74–80.
41. Chen Y, Hong F, Chen H, et al. Distinctive expression and cellular distribution of dopamine receptors in the pancreatic islets of rats. *Cell Tissue Res.* 2014;35:597–606.
42. Rubí B, Ljubicic S, Pournourmohammadi S, et al. Dopamine D2-like receptors are expressed in pancreatic β-cells and mediate inhibition of insulin secretion. *J Biol Chem.* 2005;280:36824–36832.
43. García-Tornadú I, Ornstein AM, Chamson-Reig A, et al. Disruption of the dopamine D2-receptor impairs insulin secretion and causes glucose intolerance. *Endocrinology.* 2010;151:1441–1450.
44. Simpson N, Maffei A, Freeby M, et al. Dopamine-mediated autocrine inhibitory circuit regulating human insulin secretion in vitro. *Mol Endocrinol.* 2012;26:1757–1772.
45. Sakano D, Choi S, Kataoka M, et al. Dopamine D2 receptor-mediated regulation of pancreatic β-cell mass. *Stem Cell Reports.* 2016;7:95–109.
46. Garcia Barrado MJ, Osma MCI, Blanco EJ, et al. Dopamine modulates insulin release and is involved in the survival of rat pancreatic β-cells. *PLoS One.* 2015;10: e0123197.
47. Maffei A, Segal AM, Alvarez-Perez JC, et al. Anti-incretin, anti-proliferative action of dopamine on β-cells. *Mol Endocrinol.* 2015;29:542–557.
48. Mezey E, Eisenhofer G, Harta G, et al. A novel nonneuronal catecholaminergic system: exocrine pancreas synthesizes and releases dopamine. *Proc Natl Acad Sci USA.* 1996;93:10377–10382.
49. Miller RE. Pancreatic neuroendocrinology: peripheral neural mechanisms in the regulation of the Islets of Langerhans. *Endocr Rev.* 1981;2:471–494.
50. Mignini F, Tomassoni D, Traini E, Amenta F. Dopamine, vesicular transporters and dopamine receptor expression and localization in rat thymus and spleen. *J Neuroimmunol.* 2009;206:5–13.